Oxidative Addition of Hydrogen Halides and Dihalogens to Pd. Trends in Reactivity and Relativistic Effects

G. Theodoor de Jong,[†] Attila Kovács,[‡] and F. Matthias Bickelhaupt*,[†]

Afdeling Theoretische Chemie, Scheikundig Laboratorium der Vrije Universiteit, De Boelelaan 1083, NL-1081 HV Amsterdam, The Netherlands, and Research Group of Technical Analytical Chemistry, Hungarian Academy of Sciences, Budapest University of Technology and Economics, H-1111 Budapest, Szt. Gellért tér 4, Hungary

Received: March 10, 2006

We have theoretically studied the oxidative addition of HX and X_2 to palladium for X = F, Cl, Br, I and At, using both nonrelativistic and ZORA-relativistic density functional theory at BLYP/QZ4P. The purpose is 3-fold: (i) to obtain a set of consistent potential energy surfaces (PESs) to infer accurate trends in reactivity for simple, archetypal oxidative addition reactions; (ii) to assess how relativistic effects modify these trends along X = F, Cl, Br, I and At; and (iii) to rationalize the trends in reactivity in terms of the reactants' molecular-orbital (MO) electronic structure and the H−X and X−X bond strengths. For the latter, we provide full Dirac−Coulomb CCSD(T) benchmarks. All oxidative additions to Pd are exothermic and have a negative overall barrier, except that of HF which is approximately thermoneutral and has a positive overall barrier. The activation barriers of the HX oxidative additions decrease systematically as X descends in group 17 of the periodic table; those of X_2 first increase, from F to Cl, but then also decrease further down group 17. On the other hand, HX and X_2 show clearly opposite trends regarding the heat of reaction: that of HX becomes *more* exothermic and that of X_2 *less* exothermic as X descends in group 17. Relativistic effects can be as large as 15−20 kcal/mol but they do not change the qualitative trends. Interestingly, the influence of relativistic effects on activation barriers and heats of reaction decreases for the heavier halogens due to counteracting relativistic effects in palladium and the halogens.

1. Introduction

Oxidative addition and reductive elimination (eq 1) are ubiquitous as elementary reaction steps in homogeneous catalysis[1−4] and have been intensively investigated both experimentally[4−7] and theoretically.[6,8−14]

$$ML_n + X{-}Y \underset{\text{reductive elimination}}{\overset{\text{oxidative addition}}{\rightleftharpoons}} X{-}ML_n{-}Y \qquad (1)$$

A well-known class of processes involving oxidative addition is catalytic C−X bond activation.[1,2,15] The catalytically active species in these reactions are generally coordination complexes of palladium or other transition-metals.

In the present study, we focus on the related processes of hydrogen−halide and dihalogen oxidative addition to palladium, for all halogens from fluorine to astatine (see Scheme 1). Apart from being involved in various catalytic processes,[1,16] the oxidative addition of hydrogen halides is also a model for the addition of more complex HX species in which X is, for example, formate or acetate.[17] Furthermore, the reactant (or precursor) complexes of dihalogen (in particular, I_2) complexes have been studied not only theoretically but also experimentally as models for early stages of the oxidative addition mechanism.[18]

Our purpose is, in the first place, to obtain a set of consistent potential energy surfaces (PESs), which enable us to infer accurate trends in reactivity for these simple, archetypal oxidative addition reactions. A second purpose of this study is to assess how relativistic effects affect these trends along X = F, Cl, Br, I and At. In the third place, we wish to rationalize the trends in reactivity in terms of the reactants' molecular-orbital (MO) electronic structure[19] and the H−X and X−X bond strengths. Here, it is an asset of our model systems that they are simple because this facilitates the analyses and puts emphasis on the essential features in the electronic structure. Thus, we have explored the PES for oxidative addition of HX and X_2 to palladium for X = F, Cl, Br, I and At, using both nonrelativistic and ZORA-relativistic density functional theory at BLYP/QZ4P. In the course of our work, we have also computed highly accurate full Dirac-Coulomb CCSD(T) benchmarks for H−X and X−X bond energies that take spin−orbit coupling into account. One of our findings is that, interestingly, relativistic effects on activation barriers and heats of reaction decrease for the heavier halogens. In this study, we focus on the overall reaction barrier, that is, the difference in energy between the transition state and the separate reactants, which is decisive for the rate of chemical reactions in the gas phase, in particular, if they occur under low-pressure conditions in which the reaction system is (in good approximation) thermally isolated[7,20] (see also section II of ref 21).

SCHEME 1: Model Reactions and Nomenclature (X = halogen, Y = H or X)

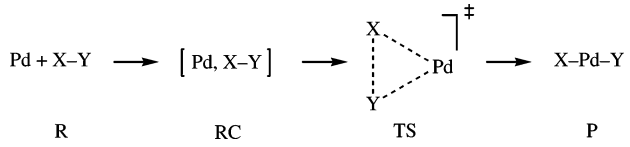

* Corresponding author. Fax: +31-20-59 87629. E-mail: fm.bickelhaupt@few.vu.nl.
† Scheikundig Laboratorium der Vrije Universiteit.
‡ Budapest University of Technology and Economics.

10.1021/jp061501v CCC: $33.50
Published on Web 06/02/2006

2. Method and Computational Details

2.1. DFT Calculations. All density functional theory (DFT)[22] calculations have been carried out with the Amsterdam Density Functional (ADF) program.[23,24] Calculations were done either nonrelativistically or with scalar relativistic effects accounted for using the zeroth-order regular approximation (ZORA).[25] For the dissociation energies of the dihalogens and hydrogen halides, where spin−orbit coupling is expected to be important, also single-point calculations using double-group symmetry including spin−orbit effects were done. The BLYP[26] density functional was used, in combination with the QZ4P basis set for all elements except hydrogen for which the TZ2P basis was used. The QZ4P basis set is a large uncontracted set of Slater-type orbitals (STOs) containing diffuse functions. It is of quadruple-ζ quality and has been augmented with several sets of polarization functions on each atom: two 3d and two 4f sets on F, three 3d and two 4f sets on Cl, two 4d and three 4f sets on Br, one 5d and three 4f sets on I, one 6d and two 5f sets on At, and two 5p and two 4f sets on Pd. The TZ2P basis set, only used for hydrogen, is of triple-ζ quality and has been augmented with two sets of polarization functions: 2p and 3d in the case of H. An auxiliary set of s, p, d, f and g STOs was used to fit the molecular density and to represent the Coulomb and exchange potentials accurately in each SCF cycle.[23] All electrons were treated variationally (i.e., no frozen-core approximation). Closed-shell and open-shell systems were treated by using the spin-restricted and spin-unrestricted formalism, respectively. The electronic structures of Pd, HX and X_2 were analyzed in terms of the quantitative molecular orbital (MO) model contained in Kohn−Sham DFT.[19] Recently, it has been shown that our approach agrees in general satisfactorily with high-level relativistic ab initio calculations for oxidative addition reactions of C−H,[10] C−C,[12] C−F,[13] and C−Cl[14] bonds to palladium.

Equilibrium and transition state geometries were fully optimized using analytical gradient techniques. All structures were verified by frequency calculations: for minima all normal modes have real frequencies, whereas transition states have one normal mode with an imaginary frequency. The character of the normal mode associated with the imaginary frequency was analyzed to ensure that the correct transition state was found. Enthalpies at 298.15 K and 1 atm were calculated from electronic energies assuming an ideal gas according to

$$\Delta H_{298} = \Delta E + \Delta E_{\mathrm{trans},298} + \Delta E_{\mathrm{rot},298} + \Delta E_{\mathrm{vib},0} + \Delta(\Delta E_{\mathrm{vib},0})_{298} + \Delta(pV) \quad (2)$$

Here, $\Delta E_{\mathrm{trans},298}$, $\Delta E_{\mathrm{rot},298}$ and $\Delta E_{\mathrm{vib},0}$ are the differences between products and reactants in translational, rotational and zero-point vibrational energy, respectively; $\Delta(\Delta E_{\mathrm{vib},0})_{298}$ is the change in the vibrational energy difference going from 0 to 298.15 K. The vibrational energy corrections are based on our unscaled frequency calculations. The molar work term $\Delta(pV)$ is $(\Delta n)RT$; $\Delta n = -1$ for two reactants (Pd + HX or Pd + X_2) combining to one species. Thermal corrections for the electronic energy are neglected.

2.2. Ab Initio Calculations. Based on the ZORA-BLYP/QZ4P optimized geometries, ab initio dissociation energies of X_2 and HX were calculated at the advanced correlated CCSD(T) level[27] with the program package DIRAC.[28] A full all-electron four component Dirac−Coulomb approach was used, which allowed nonrelativistic calculations with the Lévy−Leblond approximation[29] (designated here as CCSD(T)), relativistic calculations without spin−orbit coupling using a spin-free Dirac−Coulomb Hamiltonian[30] (SFDC−CCSD(T)), and relativistic calculations using the unmodified Dirac−Coulomb Hamiltonian, which includes spin−orbit coupling (DC−CCSD(T)). The two-electron integrals over the small components have been neglected and corrected with a simple Coulombic correction, which has been shown reliable.[31] The basis sets used were for hydrogen, fluorine and chlorine Dunning's correlation consistent augmented triple-ζ (aug-cc-pVTZ) basis sets,[32] and for bromine, iodine, and astatine Dyall's relativistically optimized triple-ζ basis sets.[33]

3. Results and Discussion

3.1. Reaction Profiles and Geometries. In this section, we discuss the fully relativistic potential energy surfaces of the various oxidative insertion reactions as well as the geometries of the stationary points, that is, all computed at ZORA-BLYP/QZ4P//ZORA-BLYP/QZ4P, designated R//R in the tables. Structural results are summarized in Figures 1 and 2 and Tables 1 and 2 and results about reaction profiles in Figure 3 and Table 3. In Tables S1 and S2 in the Supporting Information energies with zero-point vibrational energy correction and enthalpies at 298.15 K are reported. In section 3.2, we examine how relativistic effects have affected the trends in reactivity. Finally, in section 3.3, we try to understand the trends in reactivity in terms of the electronic structure of the reactants and the H−X and X−X bond strengths.

First, the oxidative addition reactions of HX + Pd are examined. They may all proceed from the reactants (R) via a reactant complex (RC) to a transition state (TS) that connects the RC with the product (P) in which the H−X bond is broken (see Figure 1 and Table 1). For all HX except HF, there is also a direct approach, perpendicularly to the H−X bond, without a barrier possible (vide infra). In the reactant complex, Pd binds to the halogen atom X with a Pd−X−H angle close to 100° for all hydrogen halides except hydrogen fluoride (see Table 1). In the case of the latter, Pd binds to the hydrogen atom and forms a linear Pd−H−X structure. The substrates HCl to HAt have a donor lone pair (LP) orbital on the halogen, which is fitted well for donation of electronic charge from the LP to the empty Pd 5s orbital, which causes Pd to bind to the halogen. The fluorine in HF is very electronegative and donates less well. Therefore, Pd will bind to the hydrogen, where it can donate electronic charge to the empty antibonding $\sigma^*_{\mathrm{H-F}}$, which is strongly located on the hydrogen. The complexation energies between Pd and HX (i.e., the energy of RC relative to R) range from −4.9 kcal/mol for HF to −20.2 kcal/mol for HAt (see Table 3, R//R data). Activation barriers and reaction energies also show a pronounced trend: both decrease systematically from X = F to At. Only Pd + HF has a positive overall barrier and is approximately thermoneutral. The other reactions have all negative overall barriers and are pronouncedly exothermic. For example, the activation energies are +11.9 (F), −10.4 (Cl), −12.7 (Br), −18.3 (I) and −18.5 kcal/mol (At) (see Table 3, R//R data).

Interestingly, the TS of Pd + HF is found to be of a different nature than the TS of the other Pd + HX reactions. For the latter, there is in fact no barrier for a direct approach of the palladium perpendicular to the H−X bond. Thus, for Pd + HCl, HBr, HI and HAt the energy increases as Pd is moving away from the equilibrium position of the RC because this weakens the coordination bond. The TS is reached as Pd is arriving at the rim of the reactive zone that surrounds the H−X bond: if Pd moves across this border, it spontaneously inserts (in a sense, it falls) into the H−X bond, which then spontaneously gives way and breaks. At variance, the TS for Pd + HF is inherently

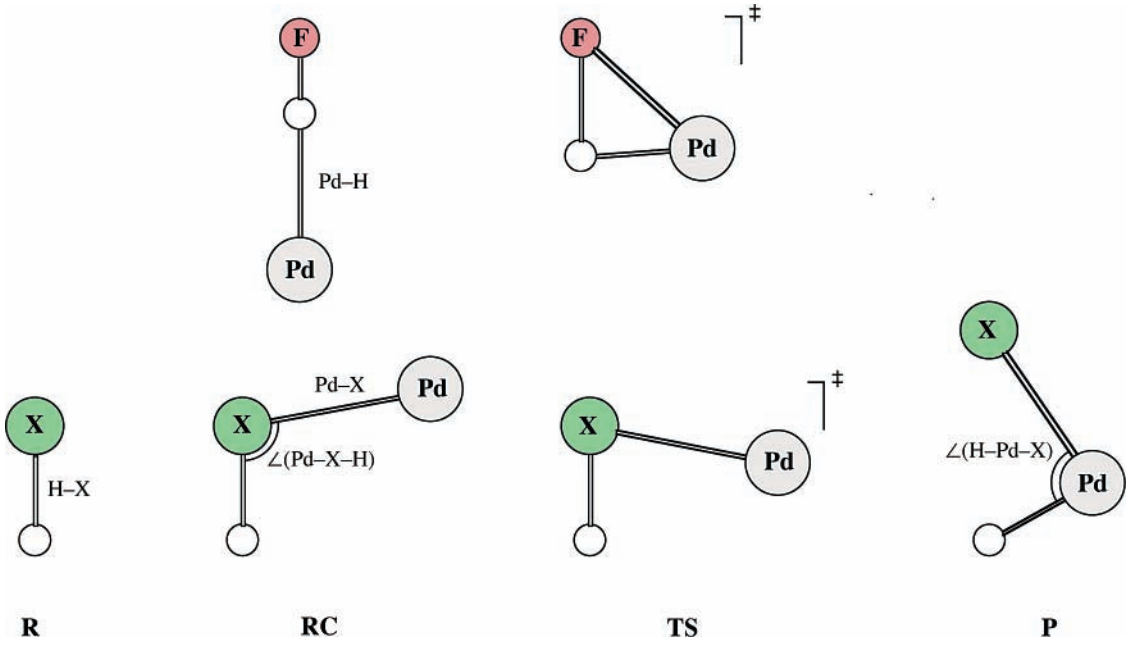

Figure 1. Structures of stationary points on the potential energy surface for the oxidative addition of Pd to hydrogen halides HX with X = F, Cl, Br, I and At (see Table 1 for values). Note that structures involving HF differ from those of other HX.

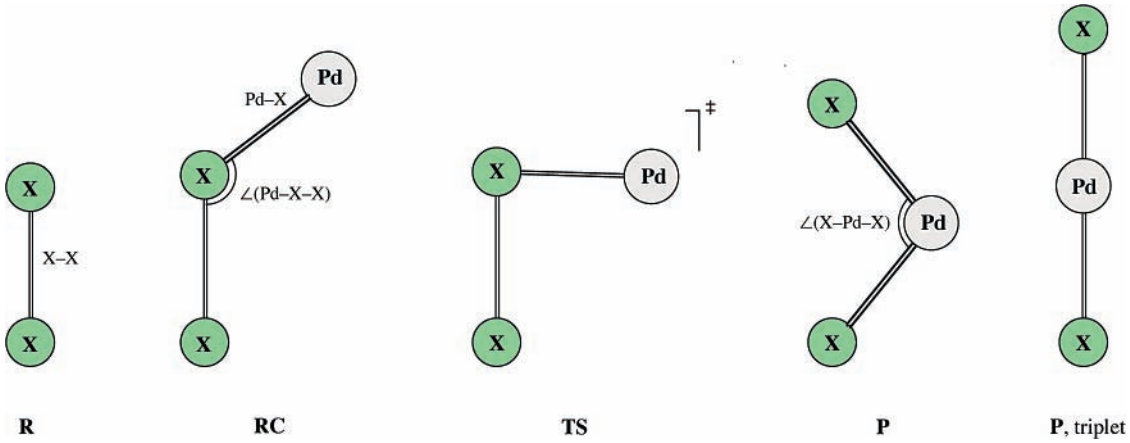

Figure 2. Structures of stationary points on the potential energy surface for the oxidative addition of Pd to dihalogens X_2 with X = F, Cl, Br, I and At (see Table 2 for values).

connected with the movement of insertion into the H−F bond and it is also present in the case of a direct approach of Pd perpendicular to the H−F bond.

Next, we inspect the oxidative addition reactions of X_2 + Pd. Similar to the situation of the hydrogen halides, the dihalogen additions may all proceed from the reactants (R) via a reactant complex (RC) to a transition state (TS) that connects the RC with the product (P) in which the X−X bond is broken (see Figure 2 and Table 2). In the reactant complex, Pd binds to the halogen atom X with a Pd−X−X angle that decreases systematically from 180° for F_2 to 113° for At_2 (see Table 2).

Regarding the energetics, there are striking differences between oxidative addition of X_2 and HX. The complexation energies between Pd and X_2 (i.e., the energy of RC relative to R) are considerably more stabilizing than in the case of Pd + HX: they range from −44.0 kcal/mol for F_2 to −29.4 kcal/mol for At_2 (see Table 3, R//R data). Activation barriers for Pd + X_2 are also generally lower than those for Pd + HX. Furthermore, the barriers of Pd + X_2 first *increase*, from X = F to Cl, but then decrease along X = Cl, Br, I and At (see Figure 3). The activation energy goes up from approximately (vide infra) −32 kcal/mol for F_2 to −22.6 for Cl_2 and, thereafter, goes down to −27.6 kcal/mol for At_2. The nature of the transition states resembles that of the corresponding Pd + HX reactions in the sense that they occur only if one proceeds from the RC while oxidative addition proceeds again barrierless if Pd approaches the dihalogen side-on, that is, perpendicular to the X−X bond. Contrary to the situation for Pd + HX, the oxidative addition of X_2 to Pd becomes systematically *less* exothermic along X = F−At (see Figure 3). Thus, the reaction energy for Pd + X_2 goes from a very exothermic −101.3 kcal/mol for X = F up to the less exothermic −49.5 kcal/mol for At (see Table 3). For comparison, in the case of Pd + HX, the reaction energy goes from approximately thermoneutral, +0.1 kcal/mol, for X = F to a clearly exothermic −40.4 kcal/mol for X = At.

Now, we come back to the barrier for Pd + F_2. The computation of an accurate value for this barrier is hampered by the fact that, only for this reaction, the triplet surface drops below the singlet one as we proceed along the reaction coordinate to the TS. This is illustrated in Figure 4, which shows the singlet and triplet PESs for Pd + F_2 (upper) and, for comparison, those for Pd + I_2 as a function of the Pd−X−X angle; the latter has been varied, in steps of 5°, from 180° (corresponding to a linear RC) to 0° (linear P) while optimizing

TABLE 1: Geometry Parameters[a] (in Å, Degrees) of Stationary Points on the Potential Energy Surface for the Oxidative Addition of HX to Pd with X = F, Cl, Br, I and At[b]

		H−X		Pd−X		Pd−H		∠(Pd−X−H)		∠(H−Pd−X)	
substrate		NR	R	NR	R	NR	R	NR	R	NR	R
H−F	R	0.934	0.935								
	RC	0.967	0.974	3.000	2.969	2.033	1.995	0.0	0.0	0.0	0.0
	TS	1.665	1.497	2.085	2.083	1.531	1.538	46.5	47.5	52.1	45.8
	P	2.468	2.487	1.966	1.925	1.525	1.511	38.2	37.4	89.0	91.6
H−Cl	R	1.291	1.291								
	RC	1.300	1.306	2.480	2.343	3.052	2.922	103.2	102.7	24.5	25.9
	TS	1.307	1.317	2.515	2.373	2.575	2.466	77.7	78.1	29.7	31.5
	P	2.532	2.627	2.284	2.236	1.528	1.511	36.5	35.0	80.6	86.8
H−Br	R	1.437	1.435								
	RC	1.451	1.458	2.553	2.439	3.221	3.103	103.7	102.6	26.0	27.3
	TS	1.457	1.467	2.577	2.461	2.650	2.575	76.6	77.4	32.3	33.8
	P	2.447	2.668	2.418	2.366	1.535	1.513	36.8	34.3	72.7	83.8
H−I	R	1.634	1.630								
	RC	1.653	1.658	2.613	2.532	3.402	3.300	103.5	101.9	28.2	29.4
	TS	1.666	1.671	2.638	2.555	2.637	2.610	71.5	72.9	36.8	37.7
	P	1.987	2.674	2.640	2.527	1.616	1.519	37.7	33.8	48.7	78.4
H−At	R	1.738	1.726								
	RC	1.758	1.759	2.675	2.619	3.474	3.397	101.2	99.9	29.8	30.7
	TS	1.773	1.769	2.697	2.635	2.672	2.705	70.0	72.8	38.5	38.7
	P	2.120	2.668	2.705	2.616	1.609	1.524	36.5	33.5	51.6	75.1

[a] See Figure 1 for definition. [b] NR = computed *non*relativistically at BLYP/QZ4P; R = computed *relativistically* at ZORA-BLYP/QZ4P.

TABLE 2: Geometry Parameters[a] (in Å, deg) of Stationary Points on the Potential Energy Surface for the Oxidative Addition of X_2 to Pd with X = F, Cl, Br, I and At[b]

		X−X		Pd−X		∠(Pd−X−X)		∠(X−Pd−X)	
substrate		NR	R	NR	R	NR	R	NR	R
F−F[c]	R	1.433	1.433						
	RC	1.787	1.822	1.978	1.945	180.0	180.0	0.0	0.0
	P	2.926	2.973	1.919	1.891	40.3	38.2	99.3	103.6
	linear P (tripl)	3.866	3.806	1.933	1.903	0.0	0.0	180.0	180.0
Cl−Cl	R	2.040	2.041						
	RC	2.257	2.269	2.331	2.257	158.6	136.4	10.5	21.9
	TS	2.302	2.351	2.333	2.241	88.7	89.6	45.2	46.6
	P	3.384	3.453	2.252	2.215	41.3	38.8	97.4	102.4
	linear P (tripl)	4.586	4.448	2.293	2.224	0.0	0.0	180.0	180.0
Br−Br	R	2.348	2.346						
	RC	2.523	2.532	2.466	2.384	139.2	126.9	20.6	27.4
	TS	2.561	2.599	2.452	2.367	88.1	87.6	47.2	49.0
	P	3.508	3.591	2.390	2.351	42.8	40.2	94.4	99.6
	linear P (tripl)	4.878	4.723	2.439	2.362	0.0	0.0	180.0	180.0
I−I	R	2.742	2.737						
	RC	2.872	2.881	2.592	2.513	123.1	116.2	30.0	34.3
	TS	2.901	2.931	2.580	2.507	87.1	85.4	50.0	52.1
	P	3.612	3.724	2.565	2.522	45.2	42.4	89.5	95.2
	linear P (tripl)	5.181	5.078	2.590	2.539	0.0	0.0	180.0	180.0
At−At	R	2.953	2.923						
	RC	3.066	3.052	2.662	2.604	116.3	113.1	34.3	36.4
	TS	3.092	3.096	2.655	2.594	86.5	84.2	51.4	53.5
	P	3.662	3.786	2.660	2.614	46.5	43.6	87.0	92.8
	linear P (tripl)	5.367	5.257	2.683	2.629	0.0	0.0	180.0	180.0

[a] See Figure 2 for definition. [b] NR = computed *non*relativistically at BLYP/QZ4P; R = computed *relativistically* at ZORA-BLYP/QZ4P. [c] No TS found because of lower-lying triplet PES; see text.

all other geometry parameters in every step (linear transit). The value of approximately −32 kcal/mol (mentioned above, in Table 3 and indicated in Figure 3) for the barrier of Pd + F_2 refers to the highest point on the linear-transit PES of the singlet spin state. However, before that point, the triplet PES, which is characterized by the absence of a reaction barrier, drops below the singlet PES. It is beyond the scope of this explorative investigation to resolve the intricate problem of how this singlet−triplet crossing affects the precise mechanism and shape of the effective PES for Pd + F_2 reaction. It is, however, instructive to compare the singlet and triplet PESs of Pd + F_2 with those of Pd + I_2. In Figure 4, it can be nicely seen that for the reaction with I_2, the triplet PES is always clearly above the singlet PES until and including the product P. Only as we proceed to a linear product geometry (∠Pd−I−I = 0°) does the triplet PES become more stable than the singlet PES. We have verified that this happens for all products of dihalogen addition but not for the hydrogen halides. The linear triplet-state products of the dihalogen reactions turn out to be approximately equally stable as (At, I) up to ca. 12 kcal/mol (F) more stable than the bent products on the singlet PES (see Table 3).

3.2. Relativistic Effects. Relativistic effects are significant, but they do not change the relative order of reactivity of HX and X_2 oxidative addition to Pd along the series of halogens. Relativistic effects can be revealed by comparing the fully

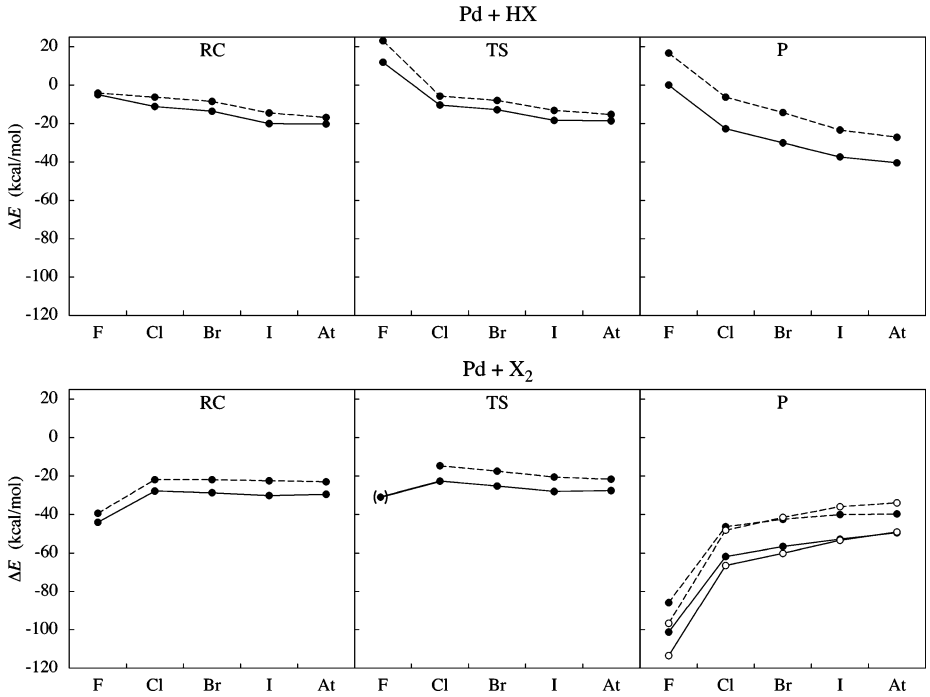

Figure 3. Relative energies (in kcal/mol) of the stationary points for oxidative addition of HX and X_2 to Pd with X = F, Cl, Br, I and At, at BLYP/QZ4P, without (dashed lines) and with ZORA relativistic effects (straight lines). For the Pd + F_2 transition state: value is an upper bound. For the Pd + X_2 product: filled circles refer to singlet states, unfilled circles to triplet states.

TABLE 3: Energies (in kcal/mol) Relative to Reactants of Stationary Points along the Potential Energy Surface for Oxidative Addition of X_2 and HX to Pd with X = F, Cl, Br, I and At[a]

	RC			TS			P			Linear P, triplet		
substrate	NR//NR	R//NR	R//R	NR//NR	R//NR	R//R	NR//NR	R//NR	R//R	NR//NR	R//NR	R//R
H−F	−4.1	−4.9	−4.9	23.1	11.3	11.9	16.7	0.5	0.1	*b*	*b*	*b*
H−Cl	−6.2	−10.3	−11.1	−5.7	−9.6	−10.4	−6.2	−22.1	−22.6	*b*	*b*	*b*
H−Br	−8.4	−12.9	−13.6	−7.8	−12.1	−12.7	−14.2	−29.0	−30.0	*b*	*b*	*b*
H−I	−14.4	−19.5	−20.0	−13.0	−17.9	−18.3	−23.3	−33.8	−37.3	*b*	*b*	*b*
H−At	−16.7	−20.0	−20.2	−15.1	−18.3	−18.5	−27.1	−38.0	−40.4	*b*	*b*	*b*
F−F	−39.3	−43.8	−44.0	*c*	*c*	(−32)[c]	−85.8	−100.7	−101.3	−96.6	−112.9	−113.3
Cl−Cl	−21.9	−26.4	−27.8	−14.7	−21.8	−22.6	−46.3	−61.2	−61.8	−48.2	−65.3	−66.5
Br−Br	−21.8	−27.7	−28.6	−17.5	−24.5	−25.1	−42.3	−56.0	−56.6	−41.4	−58.8	−60.1
I−I	−22.5	−29.4	−30.0	−20.5	−27.6	−28.0	−40.0	−52.3	−52.9	−35.9	−52.8	−53.3
At−At	−23.0	−29.2	−29.4	−21.7	−27.4	−27.6	−39.6	−49.1	−49.5	−33.8	−48.6	−49.1

[a] NR//NR = computed fully *non*relativistically at BLYP/QZ4P//BLYP/QZ4P; R//NR = energy computed *relativistically* but with *nonrelativistic geometries* at ZORA-BLYP/QZ4P//BLYP/QZ4P; R//R = computed fully *relativistically* at ZORA-BLYP/QZ4P//ZORA-BLYP/QZ4P. For definition of stationary points, see Figures 1 and 2. [b] No equilibrium structure. [c] Accurate determination hampered due to near-degeneracy of singlet and triplet PES (see text). R//R value of −32 kcal/mol is upper bound, estimated from singlet energy profile in Figure 4.

relativistic PESs discussed above (R//R data in Table 3) with the corresponding fully nonrelativistic PESs derived from nonrelativistic energies and nonrelativistic geometries of stationary points (NR//NR data in Table 3). Here, we discuss the relative electronic energy PESs summarized in Table 3. Note, however, that the PESs including zero-point vibrational energy corrections (Table S1 in the Supporting Information) and those based on relative enthalpies (Table S2 in the Supporting Information) give rise to the same trends and relativistic effects.

Relativistic effects stabilize the PES of all HX and X_2 oxidative addition reactions relative to the reactants as illustrated by the bar diagram in Figure 5. Reaction barriers are stabilized by up to 11 kcal/mol (for Pd + HF) and reactions become more exothermic by 17 kcal/mol (for Pd + HF) (see Table 3). The effect increases in most cases as one proceeds along the reaction coordinate (see Figure 5). Thus, in the case of Pd + HF, the RC, TS and P are relativistically stabilized by −0.8, −11.2 and −16.6 kcal/mol (compare R//R with NR//NR data in Table 3). One might expect relativistic effects to be more pronounced for the reactions involving the heavier halogens. This expectation is born out of the observation that relativistic effects on H−X and X−X bond strengths increase substantially along X = F, Cl, Br, I and At (vide infra; see also Table 4). Interestingly, however, the relativistic stabilization of transition states and products becomes overall smaller, not stronger, along this series in X (see Figure 5). The relativistic effects originating from the halogen atoms obviously counteract and partially cancel those originating from palladium.

Relativistic effects also affect the geometries of all species involved in the HX and X_2 oxidative addition reactions. The most striking and general effect is a shortening of the Pd−X and, in most cases, also the Pd−H bond distance (Tables 1 and 2). For example, the Pd−X distance in the transition states of Pd + HX contracts relativistically by −0.002 (F), −0.142 (Cl), −0.116 (Br), −0.083 (I) and −0.062 Å (At). Likewise, the Pd−X distance in the transition states of Pd + X_2 contracts relativistically by −0.092 (Cl), −0.085 (Br), −0.073 (I) and −0.061 Å (At). Note that the relativistic effects on geometries

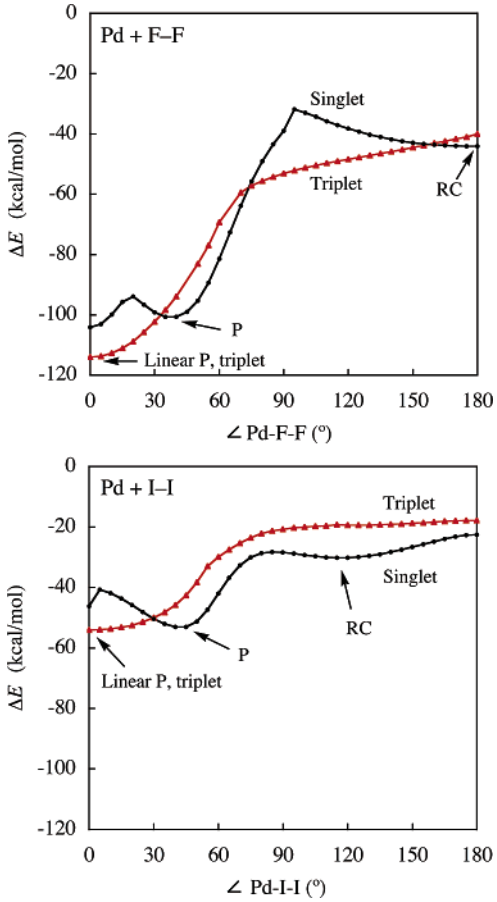

Figure 4. Energy profiles for insertion of Pd into the F−F bond and I−I bond, respectively. Singlet and triplet energies for optimized geometries at fixed Pd−X−X angle, at ZORA-BLYP/TZ2P with frozen-core approximation. An angle of 180° means a linear Pd−X−X geometry; an angle of 0° means a linear X−Pd−X geometry; see also Figure 2.

are not largest for the systems with the heaviest halogens: along Cl, Br, I and At, they even decrease systematically. This more or less parallels the trend in the relativistic effects on the activation barriers discussed above.

The above suggests that relativistic effects strengthen the Pd−substrate interaction. However, the primary effect on the energetics is not directly visible because it also induces geometrical changes that may amplify or attenuate the overall effect. To separate the initial relativistic effect on the Pd−substrate interaction from geometry relaxation effects, we have again computed all PESs at ZORA/BLYP/QZ4P//BLYP/QZ4P, that is, relativistically but with the nonrelativistic geometries (designated R//NR in Table 3). Now, it is immediately clear that the overall relativistic effects, of the order of up to 17 kcal/mol, are hardly affected by geometrical relaxation processes, which are typically in the order of 1 kcal/mol or less (they only reach larger values of 3.5 and 2.4 kcal/mol for the reaction energies of Pd + HI and Pd + HAt, respectively). In conclusion, the relativistic stabilization of RC, TS and P of the oxidative addition reactions of Pd + HX and Pd + X_2 can indeed be attributed directly to a strengthening of the Pd-substrate interaction. This is in nice agreement with similar findings for the oxidative addition reactions of Pd + CH_3X.[9]

3.3. Analysis of Trends in Reactivity and Relativistic Effects. In the previous sections, we have found, among others, that the activation barrier for HX oxidative addition decreases along X = F, Cl, Br, I and At, and that the activation barrier for X_2 oxidative addition first increases, from X = F to Cl but then decreases from X = Cl to At. We also found that relativistic effects further reduce the activation barrier for all model reactions. In this section, we try to rationalize these trends in terms of the reactants' electronic structures and the H−X and X−X bond strengths (see Figure 6 and Table 4).

The homolytic dissociation energies D_{H-X} and D_{X-X} of HX and X_2 are shown in Table 4. They have been computed both with BLYP/QZ4P and, to have an accurate benchmark, also with CCSD(T) in combination with a Gaussian triple-ζ basis set (see section 2.2 for details). Furthermore, relativistic effects have been investigated by carrying out both the BLYP and CCSD(T) computations nonrelativistically (BLYP, CCSD(T)), scalar relativistically, i.e., without spin−orbit coupling (ZORA-BLYP, spin-free Dirac−Coulomb or SFDC−CCSD(T)), and relativistically including spin−orbit coupling (SO-ZORA-BLYP, Dirac−Coulomb or DC−CCSD(T)) (see section 2.2 for details). The BLYP values agree well with those of CCSD(T) at any

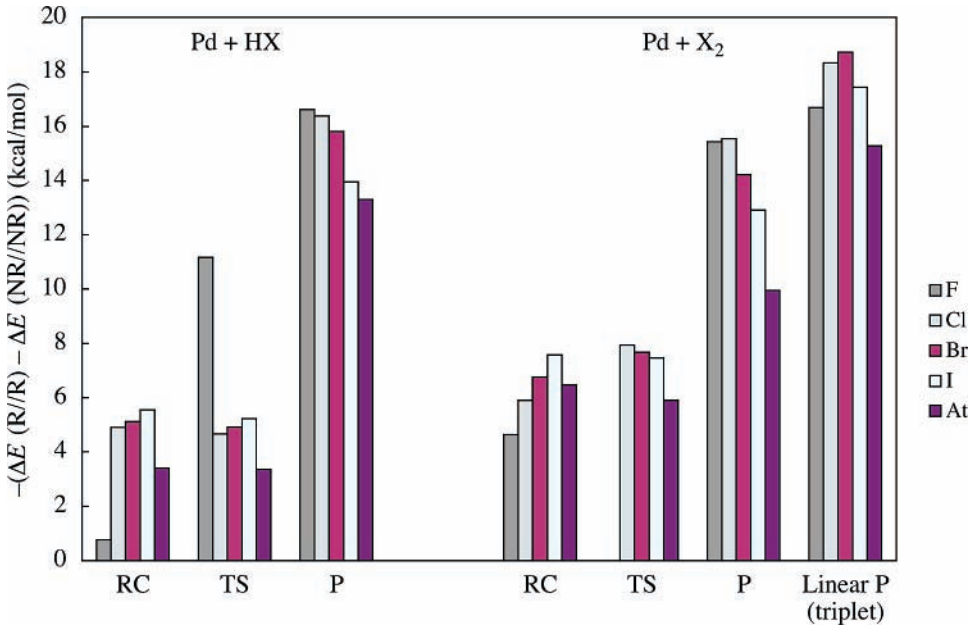

Figure 5. Relativistic effects on energies (in kcal/mol) of stationary points for the oxidative addition of HX and X_2 to Pd with X = F, Cl, Br, I and At, at BLYP/QZ4P, between nonrelativistic computations and computations with scalar relativistic effects included by ZORA.

TABLE 4: Dissociation Energies (in kcal/mol) of HX (D_{H-X}) and X_2 (D_{X-X}) for X = F, Cl, Br, I, and At, Computed at Various Levels of DFT and ab Initio Theory[a]

	D_{H-X}					D_{X-X}				
method	F	Cl	Br	I	At	F	Cl	Br	I	At
BLYP//BLYP[b]	140.9	104.5	91.5	79.5	73.9	49.0	58.1	51.6	45.8	42.9
BLYP	140.9	104.5	91.5	79.5	73.9	49.0	58.1	51.6	45.8	42.8
ZORA-BLYP	140.8	104.3	91.0	78.4	71.8	49.0	58.0	51.4	45.3	42.2
SO-ZORA-BLYP	140.7	104.0	87.5	71.3	55.5	49.0	57.5	44.9	32.4	17.5
SO-ZORA-BLYP (ΔH^{298})[c]	136.0	100.9	84.8	69.0	53.5	48.4	57.5	45.0	32.7	17.7
CCSD(T)	137.1	103.2	91.0	77.8	73.1	34.3	51.9	45.5	41.3	39.0
SFDC−CCSD(T)	136.9	103.0	90.3	76.7	70.6	34.3	51.8	45.0	40.5	36.9
DC−CCSD(T)	136.5	102.2	86.8	70.6	54.5	33.5	50.1	38.5	28.5	12.4
experiment[d]	136.4	103.2	87.5	71.3		37.9	58.0	46.1	36.1	

[a] Geometries optimized at ZORA-BLYP/QZ4P unless stated otherwise. BLYP = nonrelativistic BLYP/QZ4P. ZORA-BLYP = scalar ZORA-relativistic BLYP/QZ4P. SO-ZORA-BLYP = spin−orbit ZORA-relativistic BLYP/QZ4P. CCSD(T) = nonrelativistic CCSD(T). SFDC−CCSD(T) = CCSD(T) with relativistic spin-free Dirac−Coulomb Hamiltonian excluding spin−orbit coupling. DC−CCSD(T) = CCSD(T) with relativistic unmodified Dirac−Coulomb Hamiltonian including spin−orbit coupling. All CCSD(T) values have been counterpoise corrected (CPC) for the basis-set superposition error (BSSE). [b] Geometries optimized nonrelativistically at BLYP/QZ4P. [c] Enthalpy. [d] Obtained from corresponding enthalpies of formation at 298 K from ref 35.

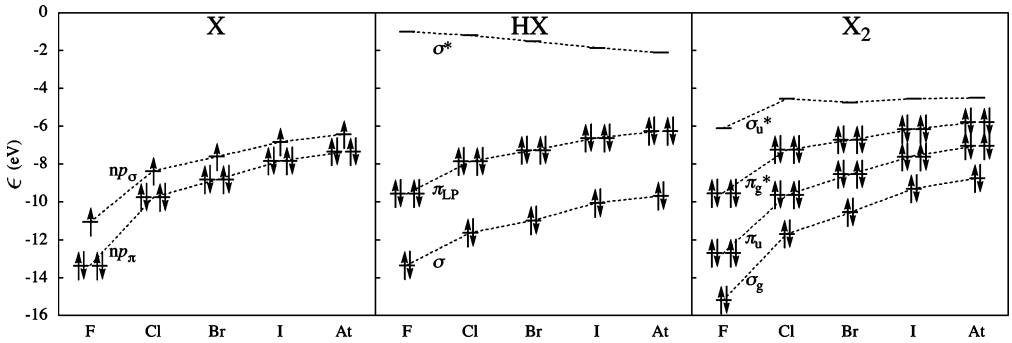

Figure 6. Orbital energies ϵ (in eV) of the frontier orbitals of X, HX and X_2 with X = F, Cl, Br, I and At, at ZORA-BLYP/QZ4P.

level of treating relativistic effects. For example, D_{H-At} amounts to 73.9, 71.8 and 55.5 kcal/mol at BLYP, ZORA-BLYP and SO-ZORA-BLYP, which agrees within 1.2 kcal/mol with 73.1, 70.6 and 54.5 kcal/mol obtained at CCSD(T), SFDC−CCSD-(T) and DC−CCSD(T), respectively, including counterpoise correction (CPC) for the basis-set superposition error (BSSE) (see Table 4). Counterpoise correction is more important for coupled-cluster calculations than for DFT calculations, as was shown in our benchmarking studies on the insertion of Pd into the C−X bond; see for example ref 14. For D_{H-X} and D_{X-X}, the BSSE can reach values of up to 3.7 kcal/mol (in case of D_{H-I}). The same trends for D_{H-X} and D_{X-X} were found in previous calculations.[34] The DC−CCSD(T) benchmark tends to yield slightly too weak bond energies (by a few kcal/mol up to 7.9 kcal/mol for Cl_2) if compared to the available experimental values.[35] Note that relativistic effects on D_{H-X} and D_{X-X} are essentially caused by spin−orbit coupling. The spin−orbit term stems from the atoms ($H^\bullet$ and $X^\bullet$, or $X^\bullet$ and $X^\bullet$) that have a doublet open-shell configuration. Spin−orbit coupling is a minor term for all closed-shell systems, Pd, HX, X_2 as well as the species at the stationary points along the PES of our model reactions. For example, the relativistic energy *with* spin−orbit coupling of the product P of Pd + At_2 relative to R is −51.2 kcal/mol (not shown in Table 3), which is only marginally different from the scalar relativistic value of −49.5 kcal/mol (see Table 3). This leads us to suggest that the scalar relativistic relative energies reported here for the stationary points for the reaction of Pd with the substrates are reliable whereas reliable dissociation energies can only be obtained if spin−orbit coupling is taken into account.

Now, we examine the trends in D_{H-X} and D_{X-X} (see Table 4). Two observations can be made: (i) the H−X bonds of the hydrogen halides (D_{H-X} = 141−56 kcal/mol at SO-ZORA-BLYP) are significantly stronger than the X−X bonds of the dihalogens (D_{X-X} = 49−18 kcal/mol at SO-ZORA-BLYP); (ii) both H−X and X−X bond strength decrease along X = F, Cl, Br, I and At, with one exception for F_2, which has a smaller bond strength than Cl_2 (vide infra). The decrease along this series is significantly more pronounced for HX than for X_2. This is so because in the former, a strong contribution to the trend is provided by the decreasing charge-stabilization that goes with the decreasing electronegativity difference across the H−X bond; this feature is completely absent in the homonuclear X_2 series. The relatively weak F−F bond originates from the very compact nature of the fluorine 2p AOs (which lack a p-type core, at variance with the np valence AOs of higher periods) as a result of which a favorable $\langle 2p_\sigma|2p_\sigma\rangle$ bond overlap occurs at a relatively short F−F distance at which there is already significant antibonding $\langle 2s|2s\rangle$ overlap (see Kovács et al.[36] for a full account of the bonding in F_2).

The above trends in H−X and X−X bond strengths contribute in a straightforward manner to the trend in the activation energies. According to the Activation Strain model[11,37] of chemical reactivity, the activation energy $\Delta E^\ddagger$ is decomposed into the activation strain $\Delta E_{strain}{}^\ddagger$ of and the stabilizing TS interaction $\Delta E_{int}{}^\ddagger$ between the reactants in the activated complex:

$$\Delta E^\ddagger = \Delta E_{strain}{}^\ddagger + \Delta E_{int}{}^\ddagger \qquad (3)$$

Here, the activation strain is entirely due to substrate bond stretching which requires more energy for HX than for X_2. Furthermore, the H−X bond strength decreases along X = F, Cl, Br, I and At whereas the X−X bond strength first increases, from X = F to Cl, and thereafter also decreases along X = Cl,

Br, I and At. This is exactly the trend in activation energies that we find for the model reactions of Pd + HX and for Pd + X_2 (see Figure 3 and Table 3−5).

The overall trend in activation energies is also dependent on the Pd−substrate interaction, that is, the TS interaction $\Delta E_{int}^{\ddagger}$, which is provided, among others, by the donor−acceptor orbital interactions between Pd 4d AOs and the substrate σ^*_{H-X} or σ^*_{X-X} LUMO. These interactions are strengthened by relativistic effects that lead to the well-known destabilization of Pd 4d AOs and thus to a smaller, more favorable HOMO−LUMO gap between Pd and the substrate (the effect is further reinforced by relativistic stabilization of the Pd 5s acceptor AO).[9] In the case of HX, the σ^*_{H-X} LUMO is mainly the 1s−np$_\sigma$ antibonding combination. The energy of this antibonding combination decreases along X = F, Cl, Br, I and At, because the np AO becomes more diffuse and, thus, the $\langle 1s|np_\sigma\rangle$ overlap smaller (see Figure 6). This reduces the HOMO−LUMO gap between Pd and HX and thus strengthens the TS interaction $\Delta E_{int}^{\ddagger}$ along this series. This further contributes to the trend of a decreasing activation energy $\Delta E^{\ddagger}$ for Pd + HX along X = F, Cl, Br, I and At (see Figure 3). In the case of X_2, the σ^*_{X-X} LUMO is mainly the np$_\sigma$−np$_\sigma$ antibonding combination. The energy of this antibonding combination *increases* along X = F, Cl, Br, I and At, because the energy of the np AO itself also increases down group 17 (see Figure 6). This causes the HOMO−LUMO gap between Pd and X_2 to become larger and thus to weaken the TS interaction $\Delta E_{int}^{\ddagger}$ along this series. From X = F to Cl, this effect enhances the trend set by the activation strain $\Delta E_{strain}^{\ddagger}$: the activation energy $\Delta E^{\ddagger}$ for Pd + X_2 increases from X = F to Cl. Thereafter, along X = Cl, Br, I and At, the trend in $\Delta E_{int}^{\ddagger}$ partially, but not completely, cancels the trend of a decreasing activation strain $\Delta E_{strain}^{\ddagger}$ for Pd + X_2 (see Figure 3). In the products, however, this effect becomes larger and does reverse the trend over the whole series. As a consequence, the reactions of Pd + X_2 become *systematically less* exothermic along X = F, Cl, Br, I and At, thus showing the opposite trend for the reaction energy as compared to Pd + HX.

Finally, note that the 2p AO of the very electronegative fluorine atom and the resulting σ^*_{X-X} LUMO of the F_2 molecule are at relatively low energy. This is the reason, in the reaction of Pd + F_2, we encounter a low-energy triplet PES. This corresponds to a single-electron transfer (SET) mechanism in which an electron has been transferred from Pd to the very low-energy σ^*_{F-F} LUMO of F_2.

4. Conclusions

The oxidative addition of both hydrogen halides (HX) and dihalogen molecules (X_2) to palladium is exothermic and goes via a negative overall barrier, except for the oxidative addition of hydrogen fluoride which is approximately thermoneutral and associated with a positive overall barrier. The activation barriers of Pd + HX decrease systematically as X descends in group 17 of the periodic table; those of Pd + X_2 increase at first, from X = F to Cl, but then decrease systematically along X = Cl, Br, I and At.

An important factor that contributes to the above trends is the strength of the H−X and X−X bonds that are broken in the process of oxidative addition: the H−X bond strength monotonically decreases along X = F, Cl, Br, I and At, whereas the X−X bond strength first increases, from X = F to Cl and thereafter decreases along X = Cl, Br, I and At. On the other hand, HX and X_2 show consistently opposite trends for the heat of reaction: that of HX becomes *more* exothermic and that of X_2 *less* exothermic as X descends in group 17. The latter is ascribed to the weakening of the Pd−substrate interaction along this series which, in the case of Pd + X_2, is strong enough to reverse the trend of decreasing X−X bond strength.

Relativistic effects reduce activation barriers and make all reactions more exothermic. This is the result of a relativistic strengthening of the Pd−substrate interaction. Interestingly, the influence of relativistic effects on activation barriers and heats of reaction decreases for the heavier halogens due to counteracting relativistic effects in palladium and the halogens.

Acknowledgment. We thank the Nederlandse Organisatie voor Wetenschappelijk Onderzoek (NWO-CW and NWO-NCF) and the Hungarian Academy of Sciences (HAS) for financial support. We thank Dr. Marcel Swart for helpful discussions.

Supporting Information Available: Tables of energies and enthalpies. This material is available free of charge via the Internet at http://pubs.acs.org.

References and Notes

(1) Collman, J. P.; Hegedus, L. S.; Norton, J. R.; Finke, R. G. *Principles and Applications of Organotransition Metal Chemistry*; University Science Books: Mill Valley, CA, 1987.

(2) Elschenbroich, Ch. A.; Salzer, A. *Organometallics: A Concise Introduction*; VCH: Weinheim, 1992.

(3) Grushin, V. V.; Alper, H. *Chem. Rev.* **1994**, *94*, 1047. Amatore, C.; Jutand, A. *Acc. Chem. Res.* **2000**, *33*, 314.

(4) Luh, T.-Y.; Leung, M.-k.; Wong, K. T. *Chem. Rev.* **2000**, *100*, 3187.

(5) Ritter, D.; Weisshaar, J. C. *J. Am. Chem. Soc.* **1990**, *112*, 6425. Fayet, P.; Kaldor, A.; Cox, D. M. *J. Chem. Phys.* **1990**, *92*, 254. Casado, A. L.; Espinet, P. *Organometallics* **1998**, *17*, 954. Stürmer, R. *Angew. Chem.* **1999**, *111*, 3509. Hinrichs, R. Z.; Schroden, J. J.; Davis, H. F. *J. Am. Chem. Soc.* **2003**, *125*, 860. de Pater, B. C.; Zijp, E. J.; Frühauf, H.-W.; Ernsting, J. M.; Elsevier, C. J.; Vrieze, K. *Organometallics* **2004**, *23*, 269. Espinet, P.; Echavarren, A. *Angew. Chem.* **2004**, *116*, 4808. Wang, G.; Chen, M.; Zhou, M. *Chem. Phys. Lett.* **2005**, *412*, 46. Lersch, M.; Tilset, M. *Chem. Rev.* **2005**, *105*, 2471.

(6) Weisshaar, J. C. *Acc. Chem. Res.* **1993**, *26*, 213. Carroll, J. J.; Haug, K. L.; Weisshaar, J. C.; Blomberg, M. R. A.; Siegbahn, P. E. M.; Svensson, M. *J. Phys. Chem.* **1995**, *99*, 13955. Porembski, M.; Weisshaar, J. C. *J. Phys. Chem. A* **2000**, *104*, 1524. Haynes, A.; Maitlis, P. M.; Morris, G. E.; Sunley, G. J.; Adams, H.; Badger, P. W.; Bowers, C. M.; Cook, D. B.; Elliott, P. I. P.; Ghaffar, T.; Green, H.; Griffin, T. R.; Payne, M.; Pearson, J. M.; Taylor, M. J.; Vickers, P. W.; Watt, R. J. *J. Am. Chem. Soc.* **2004**, *126*, 2847.

(7) Carroll, J. J.; Weisshaar, J. C. *J. Am. Chem. Soc.* **1993**, *115*, 800.

(8) Siegbahn, P. E. M.; Blomberg, M. R. A.; Svensson, M. *J. Am. Chem. Soc.* **1993**, *115*, 1952. Griffin, T. R.; Cook, D. B.; Haynes, A.; Pearson, J. M.; Monti, D.; Morris, G. E. *J. Am. Chem. Soc.* **1996**, *118*, 3029. Siegbahn, P. E. M. *J. Am. Chem. Soc.* **1996**, *118*, 1487. Wittborn, A. M. C.; Costas, M.; Blomberg, M. R. A.; Siegbahn, P. E. M. *J. Chem. Phys.* **1997**, *107*, 4318. Cui, Q.; Musaev, D. G.; Morokuma, K. *J. Chem. Phys.* **1998**, *108*, 8418. Torrent, M.; Solà, M.; Frenking, G. *Chem. Rev.* **2000**, *100*, 439. Senn, H. M.; Ziegler, T. *Organometallics* **2004**, *23*, 2980. Goossen, L. J.; Koley, D.; Hermann, H.; Thiel, W. *Chem. Commun.* **2004**, 2141. Kozuch, S.; Shaik, S.; Jutand, A.; Amatore, C. *Chem. Eur. J.* **2004**, *10*, 3072. Diefenbach, A.; Bickelhaupt, F. M. *J. Organomet. Chem.* **2005**, *690*, 2191. Diefenbach, A.; de Jong, G. Th.; Bickelhaupt, F. M. *Mol. Phys.* **2005**, *103*, 995.

(9) Diefenbach, A.; Bickelhaupt, F. M. *J. Chem. Phys.* **2001**, *115*, 4030.

(10) de Jong, G. Th.; Solà, M.; Visscher, L.; Bickelhaupt, F. M. *J. Chem. Phys.* **2004**, *121*, 9982. de Jong, G. Th.; Geerke, D. P.; Diefenbach, A.; Bickelhaupt, F. M. *Chem. Phys.* **2005**, *313*, 261.

(11) Diefenbach, A.; de Jong, G. Th.; Bickelhaupt, F. M. *J. Chem. Theory Comput.* **2005**, *1*, 286.

(12) de Jong, G. Th.; Geerke, D. P.; Diefenbach, A.; Solà, M.; Bickelhaupt, F. M. *J. Comput. Chem.* **2005**, *26*, 1006.

(13) de Jong, G. Th.; Bickelhaupt, F. M. *J. Phys. Chem. A* **2005**, *109*, 9685.

(14) de Jong, G. Th.; Bickelhaupt, F. M. *J. Chem. Theory Comput.* **2006**, *2*, 322.

(15) March, J. *Advanced Organic Chemistry*; McGraw-Hill: Tokyo, 1977. Dedieu, A. *Chem. Rev.* **2000**, *100*, 543. Nicolaou, K. C.; Bulger, P. G.; Sarlah, D. *Angew. Chem.* **2005**, *117*, 4516.

(16) Tsuji, J. *Palladium reagents and catalysts*; Wiley: Chichester, U.K., 1995. Grushin, V. V. *Chem. Rev.* **1996**, *96*, 2011.

(17) Amatore, C.; Jutand, A.; Meyer, G.; Carelli, I.; Chiarotto, I. *Eur. J. Inorg. Chem.* **2000**, 1855.

(18) Beek, J. A. M.; Koten, G. van; Smeets, W. J. J.; Spek, A. L. *J. Am. Chem. Soc.* **1986**, *108*, 5010. Koten, G. van. *Pure Appl. Chem.* **1990**, *62*, 1155. Bickelhaupt, F. M.; Baerends, E. J.; Ravenek, W. *Inorg. Chem.* **1990**, *29*, 350.

(19) Bickelhaupt, F. M.; Baerends, E. J. Kohn−Sham density functional theory: Predicting and understanding chemistry. In *Reviews in Computational Chemistry*; Lipkowitz, K. B., Boyd, D. B., Eds.; VCH Publishers Inc.: New York, 2000; Vol. 15, p 1.

(20) Nibbering, N. M. M. *Adv. Phys. Org. Chem.* **1988**, *24*, 1.

(21) Bickelhaupt, F. M. *Mass Spectrom. Rev.* **2001**, *20*, 347.

(22) Hohenberg, P.; Kohn, W. *Phys. Rev.* **1964**, *136*, B864. Kohn, W.; Sham, L. J. *Phys. Rev.* **1965**, *140*, A1133. Parr, R. G.; Yang, W. *Density-Functional Theory of Atoms and Molecules*; Oxford University Press: New York, 1989.

(23) Baerends, E. J.; Ellis, D. E.; Ros, P. *Chem. Phys.* **1973**, *2*, 41.

(24) te Velde, G.; Bickelhaupt, F. M.; Baerends, E. J.; Fonseca Guerra, C.; van Gisbergen, S. J. A.; Snijders, J. G.; Ziegler, T. *J. Comput. Chem.* **2001**, *22*, 931. Baerends, E. J.; et al. *Computer code ADF2005.01*; SCM, Theoretical Chemistry; Vrije Universiteit: Amsterdam, The Netherlands, 2005.

(25) van Lenthe, E.; Baerends, E. J.; Snijders, J. G. *J. Chem. Phys.* **1994**, *101*, 9783.

(26) Becke, A. D. *Phys. Rev. A* **1988**, *38*, 3098. Lee, C.; Yang, W.; Parr, R. G. *Phys. Rev. B* **1988**, *37*, 785.

(27) Cizek, J. *J. Chem. Phys.* **1966**, *45*, 4256. Purvis, G. D., III; Bartlett, R. J. *J. Chem. Phys.* **1982**, *76*, 1910. Raghavachari, K.; Trucks, G. W.; Pople, J. A.; Head-Gordon, M. *Chem. Phys. Lett.* **1989**, *157*, 479.

(28) Visscher, L.; Lee, T. J.; Dyall, K. G. *J. Chem. Phys.* **1996**, *105*, 8769. Aa, H. J.; Saue, J. T.; Visscher, L. *Computer code DIRAC*, release 4.0; Syddansk Universitet: Odense, Denmark, 2004.

(29) Lévy-Leblond, J. M. *Commun. Math. Phys.* **1967**, *6*, 286.

(30) Dyall, K. G. *J. Chem. Phys.* **1994**, *100*, 2118.

(31) Visscher, L. *Theor. Chem. Acc.* **1997**, *98*, 68.

(32) Kendall, R. A.; Dunning, Th. H., Jr.; Harrison, R. J. *J. Chem. Phys.* **1992**, *96*, 6796.

(33) Dyall, K. *Theor. Chem. Acc.* **2002**, *108*, 335.

(34) Visscher, L.; Dyall, K. *J. Chem. Phys.* **1996**, *104*, 9040. Visscher, L.; Styszyñski, J.; Nieuwpoort, W. C. *J. Chem. Phys.* **1996**, *105*, 1987.

(35) *NIST Standard Reference Database Number 69*, June 2005 Release; Linstrom, P. J., Mallard, W. G., Eds.; http://webbook.nist.gov/chemistry.

(36) Kovács, A.; Esterhuysen, C.; Frenking, G. *Chem. Eur. J.* **2005**, *11*, 1813.

(37) Bickelhaupt, F. M. *J. Comput. Chem.* **1999**, *20*, 114.